Improved potential energy surfaces for the interaction of H2 with Ar, Kr, and Xe

Robert J. Le Roy and Jeremy M. Hutson

Citation: J. Chem. Phys. **86**, 837 (1987); doi: 10.1063/1.452284
View online: http://dx.doi.org/10.1063/1.452284
View Table of Contents: http://jcp.aip.org/resource/1/JCPSA6/v86/i2
Published by the AIP Publishing LLC.

Improved potential energy surfaces for the interaction of H_2 with Ar, Kr, and Xe

Robert J. Le Roy
Guelph-Waterloo Centre for Graduate Work in Chemistry, University of Waterloo, Waterloo, Ontario, N2L 3G1, Canada

Jeremy M. Hutson[a)]
University Chemical Laboratory, Lensfield Road, Cambridge, CB2 1EW, England

(Received 30 December 1985; accepted 18 September 1986)

A combined analysis of discrete infrared and microwave spectra, elastic and inelastic differential cross section measurements, and virial coefficient data has been used to determine improved potential energy surfaces for the H_2–Ar, –Kr, and –Xe systems. Key improvements over previous surfaces for these species are an improved delineation of the diatom bond length dependence of the potential anisotropy, and the first experimental determination of a distinct $P_4(\cos\theta)$ anisotropy for an atom–diatom system. The effective anisotropy strength seen by bound state properties (such as transition frequencies) is found to increase from H_2–Ar to H_2–Kr to H_2–Xe, although that seen by properties sensitive to the short-range potential (such as rotational predissociation and rotational inelasticity) *decreases* along this series. This reflects the lack of conformality of the various potentials; however, both these and analogous trends predicted for properties such as vibrational frequency shifts and vibrational inelasticity are readily understood in terms of the detailed properties of these surfaces.

I. INTRODUCTION

The rare gas–molecular hydrogen interaction potentials were the first three-dimensional atom–diatom potential energy functions determined from experimental data,[1] and they remain preeminent prototype systems for the determination of anisotropic intermolecular potentials. However, the best existing potential energy surfaces for these species[2-4] are somewhat dated, both because the 15 year old spectroscopic data[5] on which they are based have been supplanted by better measurements,[6] and because they cannot fully account for the wide range of other experimental information now available. Moreover, the dispersion damping function incorporated into the long-range tails of the best existing potentials is quite simple-minded, and fails to reflect the improved understanding of the nature of van der Waals interactions achieved over the past decade.[7-14]

In recent years, new data sensitive to the H_2–rare gas interaction potentials have been obtained from a variety of experiments. The most important of these are McKellar's new higher resolution measurements of the infrared spectra of the rare gas–H_2 van der Waals molecules,[6] the hyperfine spectra of these complexes observed by Waaijer and Reuss,[15] and the elastic and rotationally inelastic differential scattering cross sections obtained by Buck and coworkers.[16-18] In addition, classical bulk properties such as second virial coefficients[19] and transport properties[20,21] have been determined, and measurements have been made of the pressure broadening and shifting of the Raman lines of H_2 in rare gases.[22] The shift of the fundamental frequency of H_2 trapped in an inert gas matrix[23] has also been investigated, as have the differences between the integral cross sections for differently oriented H_2 molecules.[24,25] The objective of the work described here is to incorporate as much as possible of the information content of these experiments into our knowledge of the potential energy surfaces for the interaction of diatomic hydrogen with Ar, Kr, and Xe.

In the following, Sec. II describes the types of data used in this analysis, the information content and the limitations of each, and the computational methods used to simulate them. Section III then describes the functional form used for the potential energy surfaces, Sec. IV outlines the fitting procedure used, and Sec. V presents the resulting surfaces and compares them to earlier potentials obtained for these species.

II. NATURE OF THE EXPERIMENTAL DATA USED IN THE ANALYSIS

The coordinates used for describing atom–diatom systems are the diatom bond length r, the distance R between the atom and the center of mass of the diatom, and the angle θ between the axes of the diatom and of the complex. Within the electronic Born–Oppenheimer approximation, an intermolecular potential expressed as a function of all three of these coordinates is appropriate for *any* isotopic species of the complex, and it is unnecessary to use separate potentials for different isotopes. To within the accuracy of the available measurements, this approximation appears to be valid for these systems.

The intramolecular dynamics and interaction potential actually depend on all three degrees of freedom. However, because the frequency of the H_2 stretching vibration is an order of magnitude larger than those of the other internal motions of the complex, it is often qualitatively appropriate to think of the system as moving on a two-dimensional vibrationally averaged potential surface associated with a particular vibration–rotation (v, j) state of a given diatom isotope.

[a)] Stokes Research Fellow, Pembroke College, Cambridge. Present address: Department of Chemistry, University of Durham, Science Laboratories, South Road, Durham, DH1 3LE, England.

 0021-9606/87/020837-17$02.10

Such effective potentials may be expanded as Legendre series

$$\overline{V}_{vj}(R,\theta) = \overline{V}_0(R) + \overline{V}_2(R)P_2(\cos\theta), \quad (1)$$

where $\overline{V}_0(R)$ and $\overline{V}_2(R)$ are the vibrationally averaged isotropic and anisotropic radial strength functions for that v,j and diatom isotope. While a more detailed description of the potential form is presented in Sec. III, Eq. (1) provides a useful basis for a discussion of the information content of the various types of data.

A. Infrared spectra of the van der Waals molecules

The discrete infrared spectra of the rare gas–H_2 van der Waals molecules are the most potent single source of information on their potential energy surfaces. The complexes are weakly bound, with well depths of only 50–65 cm^{-1} and zero point energies (for the H_2 species) of $\sim 30\,cm^{-1}$. They are all weakly anisotropic systems whose eigenstates are characterized by quantum numbers associated with the total angular momentum (J), the diatom vibration and rotation (v and j), the end-over-end angular momentum of the complex (l), and the stretching vibration of the van der Waals bond (n). While the only rigorously conserved quantities are the total angular momentum (J) and the parity $(-1)^{j+l}$, the other quantum numbers are also nearly exact. The observed infrared transitions all correspond to $v = 0 \rightarrow 1$ and $\Delta j = 0$ or 2. The bands are therefore identified by the usual label for the associated free diatom transition [e.g., $Q_1(0)$ for $v = 0 \rightarrow 1, j = 0 \rightarrow 0$, or $S_1(1)$ for $v = 0 \rightarrow 1$, $j = 1 \rightarrow 3$], while the individual lines are labeled by the changes in and initial value of l [e.g., $T(3)$ identifies a transition in which l changes from 3 to 6].

All of the assigned lines in the infrared spectra involve transitions between levels corresponding to van der Waals bond stretching quantum number $n = 0$, but the end-over-end rotational (l) levels are followed all the way to dissociation. The associated rotational spacings and centrifugal distortion effects comprise the principal source of information about the wells of the effective isotropic (spherically averaged) potentials. When combined with theoretical knowledge of the limiting long-range behavior of these potentials,[26] they allow a fairly precise determination of the shapes of these functions in the well region.

The infrared spectra are the only source of information about the dependence of the effective isotropic radial potentials on the hydrogen bond length r. This sensitivity arises because the stretching of the diatom bond associated with its vibrational and/or rotational excitation gives rise to differences among the effective potentials for complexes formed from H_2 or D_2 in different internal states. These differences manifest themselves as red shifts of the band origins of the complex relative to the associated free monomer level spacings. Moreover, this degree of freedom is only very weakly correlated with the dependence of the potential on R. The available data involve complexes formed from H_2 and D_2 in $v = 0$ and 1, with bond lengths $\langle r \rangle_{vj}$ differing by only 8.6%. However, additional information on the stretching dependence is provided by the collapsed diatom limit constraint discussed in Sec. III, and by the fact that the stretching dependence of the C_6 dispersion constants is known from theory.[26]

The anisotropy of the potential affects the infrared data by splitting and shifting the l levels of complexes correlating with rotationally excited hydrogen into components associated with different values of J. These shifts are of the order of 0.5 cm^{-1}, and are effectively determined by the expectation value of the anisotropy strength function $\overline{V}_2(R)$ over bound state radial wave functions such as ψ_b or ψ_m in Fig. 1. For the ground state of H_2–Ar, the integrand of this expectation value is shown in the bottom segment of Fig. 2; it has its maximum in the well region near 3.8 Å and is only weakly dependent on the strength of the anisotropy at distances shorter than $\sigma = 3.18$ Å. Since these expectation values do not change very dramatically with l, the observed shifts alone do not provide a very accurate determination of the shape of the $\overline{V}_2(R)$ function(s). The resulting model dependence is clearly illustrated by the fact that equally good fits to the old[5] H_2– and D_2–Ar data using different potential models yielded anisotropy strength scaling parameters differing by up to 28%! While this type of model dependence also intrudes on our determination of other features of the potential, its depradations are most serious for the anisotropy and (particularly) for its diatom bond-length dependence. It is their improved ability to reduce this model de-

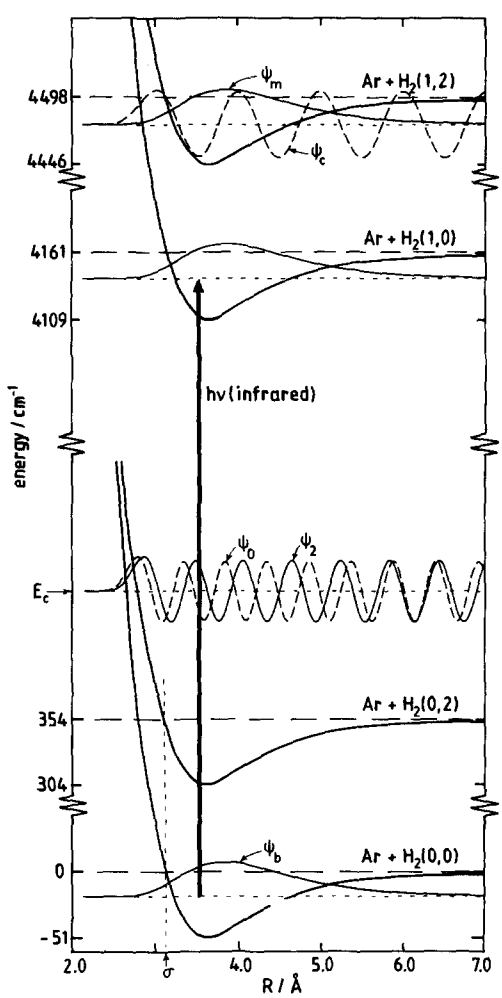

FIG. 1. Illustration of the nature of the wave functions of states involved in the phenomena of interest.

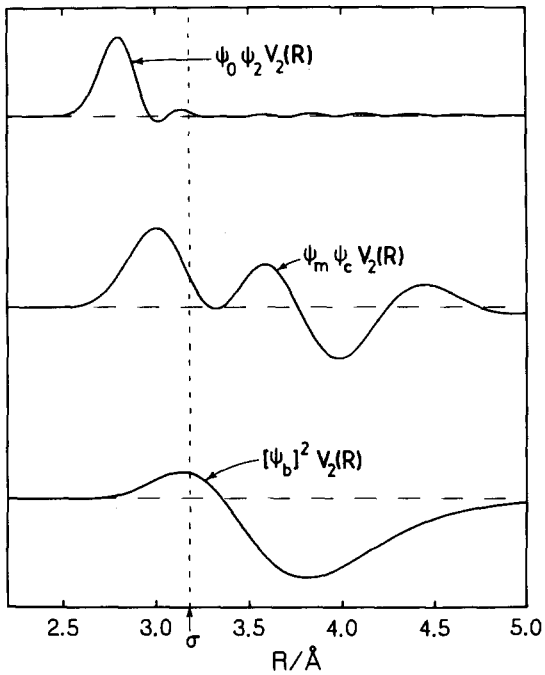

FIG. 2. Integrands of matrix elements governing the influence of the potential anisotropy on bound state properties (lowest curve), on rotational predissociation (middle curve), and on rotational inelasticity (uppermost curve).

pendence that makes the new higher resolution infrared data[6] so valuable.

The main limitations on the information obtainable from the infrared spectra are the model dependence mentioned above and the insensitivity of the data to the potential at van der Waals distances smaller than the zero of the effective isotropic potential (at $R = \sigma$), where the bound state radial wave functions rapidly die off (see Figs. 1 and 2). As more accurate experimental data become available, the model dependence will decrease and the resulting potentials will extrapolate more reliably to smaller distances. However, model dependence may also be reduced by including in the analysis the other properties discussed below.

In the present work, the method used for calculating the infrared transition frequencies and widths from a given trial potential was the secular equation/perturbation theory (SEPT) method of Ref. 27. This is an essentially exact procedure which does not rely on the qualitative arguments used above. However, those arguments are still useful for illustrating the information content of the data.

B. The hyperfine spectra

For complexes of ortho-H_2 with Ne, Ar, and Kr, hyperfine transitions at radio frequencies have been observed by Waaijer and Reuss.[15] In the absence of potential anisotropy, these frequencies would be accurately predicted by a vector coupling model depending only on angular momentum considerations and the (known) hyperfine constants of molecular hydrogen.[28] However, the potential anisotropy mixes the zero-coupling l levels and shifts the observed frequencies away from the predictions of the vector model.

Perturbation theory arguments[29] show that these shifts are a direct reflection of the magnitude of the matrix elements of the effective anisotropy strength function $\overline{V}_2(R)$ between radial wave functions associated with end-over-end rotation quantum numbers l differing by 2. Since the centrifugal distortion of these complexes is fairly small at low l, the quantity determined is essentially the expectation value of $\overline{V}_2(R)$ for a given l level of a complex formed from ground state ortho hydrogen ($v = 0, j = 1$). The integrand of this expectation value is qualitatively the same as that associated with the anisotropic shifts in the infrared spectra (illustrated for H_2–Ar in the lowest segment of Fig. 2).

Like the infrared spectra, the hyperfine transitions are most sensitive to the anisotropy strength function in the region around 4 Å, and they are relatively insensitive to its behavior at distances shorter than $\sigma = 3.18$ Å. However, the hyperfine spectra define the expectation value of $\overline{V}_2(R)$ with an uncertainty of only 1%, which is much better than is achieved with even the new[6] infrared data. Even more important is the fact that the hyperfine data depend only on the effective anisotropy for complexes formed from hydrogen in its ground vibrational state, while the infrared spectra are most sensitive to the anisotropy for the vibrationally excited (and hence stretched) diatom. Indeed, in the infrared spectra only the $Q_1(1)$ band and the few uniquely assigned and unblended $S_1(1)$ transitions contain information on the anisotropy for $v = 0$ complexes, and this is highly correlated with information about the stretching dependence of the anisotropy. The combination of hyperfine data with infrared data is therefore important for ensuring a reliable determination of the stretching dependence of the anisotropy.

As for the infrared spectra, the calculated hyperfine frequencies used in the present work were obtained using the (essentially exact) secular equation/perturbation theory method of Ref.27.

C. Differential scattering cross sections

The only direct information on the potential at distances $R < \sigma$ comes from the total elastic and rotationally inelastic differential cross sections measured by Buck *et al.*[17,18] for D_2 scattered from Ar. (Unfortunately, such data are not yet available for H_2 or D_2 scattered from Kr or Xe.) The elastic cross sections sample the potential across the whole of the classically allowed region to the right of the turning point at the collision energy E_c (see Fig. 1). It was shown in Ref. 18 that the isotropic part of the best previous spectroscopic potential (that of Ref. 3) is in reasonable accord with the elastic differential cross-section data, and it was found here that any potential which provided a good fit to the infrared data also gave a good account of the elastic cross sections. In view of both the quality of this agreement and the relative complexity of the calculations required to simulate the scattering measurements, these data have *not* been incorporated directly into the fitting procedure. Rather, potentials determined from the other properties were tested for their ability to reproduce the differential elastic cross sections.

In contrast, the inelastic cross sections were quite poorly predicted by the earlier (purely spectroscopic) potentials; these data have therefore been included in the present analysis more directly. The inelastic cross sections provide a direct

measure of the potential anisotropy in the short range region to which the bound state spectra are relatively insensitive. The reason for these different sensitivities is illustrated by Fig. 1 and the top segment of Fig. 2. The two continuum wave functions shown in Fig. 1, ψ_0 and ψ_2, are eigenfunctions associated with the collision of ground state ($j=0$) and rotationally excited ($j=2$) D_2 with Ar at $E_c = 85$ meV. Within the distorted wave Born approximation, the inelastic cross section is proportional to the square of the matrix element of the effective potential anisotropy $\overline{V}_2(R)$ involving these two wave functions. The integrand of this matrix element is shown in the top section of Fig. 2; this function peaks sharply near the classical turning point of the isotropic potential at the energy in question. Although the partial wave sum makes this apparently very local sensitivity somewhat more diffuse, these cross sections are still much more sensitive to the short range anisotropy than are the bound state data characterized by the integrand shown in the bottom segment of Fig. 2.

On the basis of similar considerations, Buck *et al.*[18] characterized the strengths of the anisotropies of different D_2–Ar potentials in terms of the strength of $\overline{V}_2(R)$ at a distance $R = 2.7$ Å, which lies near the inner turning point of the effective isotropic potential at the experimental energy E_c. We therefore included a value of $\overline{V}_2$ (2.7 Å) as a pseudo-experimental datum in the fit to the spectroscopic data, and varied it manually until the resulting surface gave inelastic cross sections in good agreement with experiment. For the isotropic potentials obtained in the present work, a value of $\overline{V}_2$ (2.7 Å) = 164 ($\pm$ 2) cm^{-1} gave good agreement with the D_2 + Ar data; however, this quantity is somewhat model dependent, and any significant changes in the isotropic part of the H_2–Ar surface would require a redetermination of the "optimum" value of $\overline{V}_2$ (2.7 Å).

While not ideal, this procedure exploits the information contained in the inelastic cross sections without requiring the relatively expensive calculations needed to simulate them at every stage of our multiparameter fits. Because the quality of the fit to the other data for this system is unaffected by any reasonable choice of $\overline{V}_2$ (2.7 Å), this approach is effectively equivalent to including the inelastic cross sections directly in the analysis.

The programs required to compute the differential cross sections at the coupled states level and to perform the proper averaging over the experimental conditions[16–18] were generously supplied to us by Professor U. Buck. The calculated elastic and inelastic cross sections described here are thus directly comparable with those described in Ref. 18.

D. Rotational predissociation level widths

Rare gas–H_2 van der Waals molecules in which the H_2 component is rotationally excited can predissociate by converting internal rotational energy of the diatom into relative translational energy of the fragments.[4,30] This process is illustrated in the uppermost portion of Fig. 1, where ψ_m represents the radial wave function of the metastable predissociating ($v=1, j=2$) state, and ψ_c represents the continuum eigenfunction of the separating fragments (with H_2 in $v=1$, $j=0$) at the same energy. Within a Golden Rule treatment, the predissociation rate, which is directly proportional to the level width, varies as the square of the matrix element of $\overline{V}_2(R)$ between ψ_m and ψ_c. The integrand of this matrix element is seen in the middle section of Fig. 2; it shows that this property is more sensitive to the short range anisotropy than are the bound state level energies, although it does not probe as far into the repulsive region as do the rotationally inelastic cross sections. On the other hand, predissociation level widths have an advantage over inelastic cross sections in that they are a property of a single quantum state rather than a sum of contributions for a range of partial waves. This makes them less expensive to simulate, and removes the model-dependence introduced by the extra layers of averaging (over partial waves and the finite energy and angular resolution) associated with the scattering measurements. Predissociation lifetime measurements are therefore complementary to the infrared and hyperfine transition frequency data, so their inclusion in the analysis should lead to a substantially improved delineation of the short-range part of the potential anisotropy.

For H_2– and D_2–Ar, the rotational predissociation widths of the observed lines are both predicted[30,31] and found[6] to be too narrow to be measured. Well defined widths of a number of rotationally predissociating states *have* been measured for HD–Ar,[6] but in that case the potential term responsible for the coupling is the odd anisotropy $\overline{V}_1(R)$ component which is an artefact of the coordinate transformation associated with the displacement of the HD center-of-mass from the middle of the diatom bond. As a result, the measured widths depend mainly on the isotropic potential and its derivatives.[31,32] This portion of the potential undergoes little change in the present work, and predictions based on the existing potential[30,31] are already in good agreement with experiment.[6] Since the calculations are considerably more expensive than those for the H_2 and D_2 systems, there seemed little point in including these data in the present analysis.

For H_2–Kr, one line in the $S_1(0)$ spectrum was predicted[30] to be twice as broad as any of the others, and was found[6] to be significantly broader than the instrumental width. Unfortunately, we were unable to separate the instrumental and pressure broadening contributions to the linewidths with sufficient accuracy to obtain a reliable experimental predissociation level width for inclusion in the present analysis. However, the width of this line still provides a useful consistency test for the anisotropy of any proposed surface for this species, and measurement of more accurate values of such widths promises to be a powerful tool for determining potential anisotropies.

E. Virial coefficients

Second virial coefficients for H_2–Ar mixtures have been measured by Brewer and Vaughn and by Schramm *et al.*, while results for H_2–Kr and H_2–Xe have been reported by Brewer and by Pérez *et al.*[19] Low temperature virial coefficients contain information on the volume or capacity of the well portion of the potential energy surface,[33] whereas high temperature data are sensitive mainly to the position of the

repulsive wall. The calculations of virial coefficients, including translational and rotational quantum corrections, were performed with Pack's program,[34] using the full potential vibrationally averaged over the diatom ground ($v=0$, $j=0$) state.

F. Relevant data omitted from the analysis

For various reasons, the data for a number of other types of experiments were not exploited in the present analysis. In particular, while the transport properties and Raman line shape data are sensitive to the potential,[20–22,33,35] the calculations required to generate these properties from a given trial potential are much too expensive to be incorporated into an iterative multiparameter fitting procedure.[35] However, simulations of these properties are being used[36] to test the quality of the present optimized potentials.

The shifts in the level spacings of molecular hydrogen trapped in an inert gas matrix[23] are also potentially valuable, since they constitute one of the few properties directly sensitive to the dependence of the intermolecular potential on the diatom bond length. However, a generally reliable methodology for calculating such shifts has not yet been established, and the interpretation of the experimental data is complicated by the presence of many-body interactions, about which little is known. These data were therefore omitted from consideration here.

The integral cross section anisotropy measurements of Zandee and Reuss[25] were also excluded from the present analysis. The earlier analysis of their data was based on distorted wave calculations, which in themselves are moderately expensive. However, because the measurements span the orbiting resonance region where distorted wave techniques are known to be unreliable,[35,37] much more expensive computational procedures would be necessary to ensure reliability. Moreover, the most appropriate way of accounting for the averaging over apparatus parameters and experimental conditions is not entirely clear. At the same time, within mutual uncertainties, the (more precisely defined) potential anisotropy parameters determined here agree with those reported in Ref. 25, so there seemed to be little point in explicitly including these data in the present study.

III. THE POTENTIAL FORM

A. General

As in previous work,[1–3] the angle and diatom stretching dependence of the potential was represented by the double linear expansion:

$$V(R,\xi,\theta)=\sum_k\sum_\lambda \xi^k P_\lambda(\cos\theta)V_{\lambda k}(R), \tag{2}$$

where the diatom stretching coordinate is defined as $\xi=(r-r_0)/r_0$, with r_0 fixed at the expectation value of r for the ground state of H_2, $r_0=0.766\,639\,3$ Å. The radial strength functions $V_{\lambda k}(R)$ were again chosen to have the damped exponential-(6,8) form

$$V_{\lambda k}(R) = A\exp(-\beta R)-D_6(R)C_6/R^6-D_8(R)C_8/R^8. \tag{3}$$

In the present work, however, the damping functions $D_6(R)$ and $D_8(R)$ differ from those used earlier, both in their analytic form and in the fact that they are different from one another.

In practice, the nature of the damping functions used in Eq. (3) is not important, since both the fits to the data and most properties of the resulting potentials are insensitive to this subtlety of the potential form. However, the Buckingham–Corner form used previously[1–4] was an *ad hoc* function devised solely to remove the singularity of the inverse-power dispersion terms at $R=0$. It has discontinuous derivatives at the potential minimum (where it is "turned on"), and it gives a very poor representation of the directly calculated dispersion energy damping for certain simple systems.[38]

Various procedures for circumventing these deficiencies have been proposed[7–14]; in the present work, we chose to use the incomplete gamma function damping functions proposed by Tang and Toennies[14]:

$$D_n(R)=P(n+1,\beta R)=1-e^{-\beta R}\sum_{m=0}^{n}(\beta R)^m/m!, \tag{4}$$

where β is the exponent parameter associated with the repulsive part of $V_{00}(R)$. This function has no discontinuous derivatives, has the correct analytic behavior as $R\to 0$ and $R\to\infty$, and it reproduces the known[38] dispersion energy damping for the $^3\Sigma_u^+$ state of diatomic hydrogen. The present potentials will be referred to as "TT_3" potentials, to indicate that they use Tang–Toennies damping functions and to distinguish them from the BC_1 and BC_3 forms used previously (which used Buckingham–Corner damping functions). As before, the subscript 1 or 3 indicates the maximum value of k appearing in the polynomial expansion for the stretching dependence in Eq. (2).

The radial strength functions of Eq. (3) may be characterized by the values of the linear parameters A, C_8 and C_6 and of the exponent parameter β. However, in least-squares fits, the interparameter correlation is greatly reduced and the convergence properties of the fits greatly improved if the independent fitting variables are chosen to be the depth ϵ and position R_e of the minimum of $V_{\lambda k}(R)$, rather than A and C_8.[39] The values of A and C_8 are then defined in terms of ϵ, R_e, C_6, and β by the expressions

$$A=\{\epsilon(\mathbf{D}_8^*R_e-8)+[\mathbf{D}_6^*R_e-\mathbf{D}_8^*R_e+2]C_6\mathbf{D}_6/R_e^6\} \times\exp(\beta R_e)/(8-\beta R_e-\mathbf{D}_8^*R_e) \tag{5}$$

$$C_8=[A\exp(-\beta R_e)+\epsilon-C_6\mathbf{D}_6/R_e^6]R_e^8/\mathbf{D}_8, \tag{6}$$

where

$$\mathbf{D}_n=D_n(R=R_e)\text{ and }\mathbf{D}_n^*=[dD_n(R=R_e)/dR\,]/\mathbf{D}_n.$$

In general, the parameters $\{A, C_8, C_6, \text{and } \beta\}$ or $\{\epsilon, R_e, C_6, \text{and } \beta\}$ are all different for each (λ,k) pair. This is certainly true for the first three, and in principle could also be true for the exponent parameter β. However, even for the case of H_2–Ar, where the availability of both spectroscopic data and elastic and inelastic scattering cross sections should provide the most sensitive test of the short range potentials, we have found it unnecessary to use more than a single β

value. For each system, therefore, $\beta^{\lambda k}$ was taken to have the same value for all $\{\lambda,k\}$, and was denoted by the common symbol β.

An additional constraint applied to all three surfaces was to define R_e^{21} by the constraint $R_e^{21}/R_e^{20} = R_e^{01}/R_e^{00}$, since the fits for all three systems proved to be insensitive to this parameter.

B. Constraints on the long-range behavior

While calculated values of molecular properties are often quite sensitive to the assumed value of the asymptotically dominant C_6 potential energy coefficient, this sensitivity is rarely sufficient to allow reliable values of C_6 coefficients to be determined from experimental data. This is the case in the present study, so the $C_6^{\lambda k}$ values appearing in all of the present $V_{\lambda k}(R)$ functions were fixed at values determined from fits to theoretical dispersion energies calculated by Thakkar[26] for inert gas atoms interacting with H_2 for a variety of diatom bond lengths and relative orientations. The coefficients used here are the same as in Refs. 2–4; they are listed, together with the new values of the other potential parameters, in Table I.

C. Diatom stretching dependence and the "collapsed diatom limit"

As its bond length r approaches zero ($\xi \to -1$), an H_2 molecule becomes electronically identical to a ground state He atom. In this limit, the isotropic part of the potential energy surface between H_2 and a rare gas atom becomes the

TABLE I. Parameters defining the recommended TT_3 potential energy surfaces for H_2 or D_2 interacting with Ar, Kr, and Xe. Quantities in parentheses are the 95% confidence limit uncertainties in the fitting variables; parameters with no uncertainties are defined by some external or internal constraint (see the text). Note that the exponent parameter $\beta^{\lambda k} = \beta^{00}$ for all $\{\lambda,k\}$.

Parameter	H_2,D_2–Ar	H_2,D_2–Kr	H_2,D_2–Xe
$\epsilon^{00}/\text{cm}^{-1}$	51.069(0.68)	58.990(0.79)	64.96(1.44)
$R_e^{00}/\text{Å}$	3.581 71(0.0071)	3.718 96(0.0078)	3.9387(0.014)
$\beta^{00}/\text{Å}^{-1}$	3.5815(0.046)	3.4892(0.049)	3.503(0.113)
$C_6^{00}/\text{cm}^{-1}\,\text{Å}^6$	134500	190300	268200
$C_8^{00}/\text{cm}^{-1}\,\text{Å}^8$	1202347	1893412	3317185
A^{00}/cm^{-1}	18778229	24874365	58001041
$\epsilon^{01}/\text{cm}^{-1}$	33.57(0.46)	43.38(0.60)	56.14(1.37)
$R_e^{01}/\text{Å}$	3.7656(0.0093)	3.8427(0.010)	4.011(0.025)
$C_6^{01}/\text{cm}^{-1}\,\text{Å}^6$	115800	167300	247500
$C_8^{01}/\text{cm}^{-1}\,\text{Å}^8$	1077814	1700086	3401228
A^{01}/cm^{-1}	22164142	26831586	63468092
$\epsilon^{02}/\text{cm}^{-1}$	0.810 028	1.332 358	4.610 352
$R_e^{02}/\text{Å}$	4.556 908	4.5497 34	4.437 439
$C_6^{02}/\text{cm}^{-1}\,\text{Å}^6$	3051	5565	11710
$C_8^{02}/\text{cm}^{-1}\,\text{Å}^8$	216490	347902	1133090
A^{02}/cm^{-1}	8233817	8959229	23890715
$C_6^{03}/\text{cm}^{-1}\,\text{Å}^6$	−25270	−36890	−55800
$\epsilon^{20}/\text{cm}^{-1}$	6.0812(0.057)	7.6664(0.20)	9.819(0.61)
$R_e^{20}/\text{Å}$	3.746 16(0.012)	3.827 34(0.026)	3.886(0.14)
$C_6^{20}/\text{cm}^{-1}\,\text{Å}^6$	13500	19450	28550
$C_8^{20}/\text{cm}^{-1}\,\text{Å}^8$	319951	481378	645103
A^{20}/cm^{-1}	4212302	5020105	7999909
$\epsilon^{21}/\text{cm}^{-1}$	11.71(1.35)	15.562(0.73)	18.24(3.5)
$R_e^{21}/\text{Å}$	3.938 493	3.954 686	3.957 333
$C_6^{21}/\text{cm}^{-1}\,\text{Å}^6$	29600	43250	65120
$C_8^{21}/\text{cm}^{-1}\,\text{Å}^8$	948287	1291247	1212902
A^{21}/cm^{-1}	15411411	15406618	18111805
$\epsilon^{22}/\text{cm}^{-1}$	4.035 136	5.082 939	3.998 486
$R_e^{22}/\text{Å}$	4.141 310	4.156 413	4.230 521
$C_6^{22}/\text{cm}^{-1}\,\text{Å}^6$	5705	8624	13860
$C_8^{22}/\text{cm}^{-1}\,\text{Å}^8$	628336	809868	567799
A^{22}/cm^{-1}	11199109	10386514	10111895
$C_6^{23}/\text{cm}^{-1}\,\text{Å}^6$	−10395	−15176	−22710
$C_8^{40}/\text{cm}^{-1}\,\text{Å}^8$	...	11564(3900)	...
$C_8^{41}/\text{cm}^{-1}\,\text{Å}^8$	...	11564	...
RMSD	0.609	0.587	1.210

analogous (known[40,41]) one-dimensional He–rare gas potential curve, while the potential anisotropies become identically zero. For the C_6 constants, convincing evidence of the validity of this approach is provided by the manner in which Thakkar's[26] calculated values of $C_6^{\lambda}(\xi)$ for various H_2–M complexes approach the corresponding He–M constants as $\xi \to -1$ (see Fig. 5 of Ref. 3). Accordingly, the fits which determined the $C_6^{\lambda k}$ values were constrained to reproduce the known C_6 values for the He–inert gas pairs[42] in the collapsed diatom limit.

The available data for the H_2-inert gas systems relate to interactions involving molecular hydrogen in either $v = 0$ or 1, and the associated range of diatom bond lengths is too small to allow more than a linear dependence on ξ to be determined directly from experiment. Following Ref. 3, the "collapsed diatom limit" behavior described above was therefore imposed on the overall potential energy surface as a means of improving our knowledge of this ξ dependence. For the C_6 dispersion constants, this constraint was incorporated into the definition of the $C_6^{\lambda k}$ constants, as described above. For A and C_8, the constraint was used to define the values of the $k = 2$ radial strength function parameters in terms of those for $k = 0$ and 1, as

$$A(\text{He–M}) = A^{00} - A^{01} + A^{02},$$
$$C_8(\text{He–M}) = C_8^{00} - C_8^{01} + C_8^{02} \tag{7}$$

for $\lambda = 0$, and

$$A^{\lambda 0} - A^{\lambda 1} + A^{\lambda 2} = 0,$$
$$C_8^{\lambda 0} - C_8^{\lambda 1} + C_8^{\lambda 2} = 0 \tag{8}$$

for all $\lambda \neq 0$, where A(He–M) and C_8(He–M) are values for He–M determined from Eqs. (5) and (6) using the most recent[41] ϵ(He–M) and R_e(He–M) values (see Table II). Thus, while the sum over k in Eq. (2) runs from 0 to 3, the $k = 3$ contributions consist of only the $D_6(R)C_6/R^6$ term.

One consequence of using the above constraint is that, while the radial strength functions $V_{\lambda k}(R)$ may in principle be described using either of the parameter sets $\{\epsilon^{\lambda k}, R_e^{\lambda k}, C_6^{\lambda k}, \text{and } \beta^{\lambda k}\}$ or $\{A^{\lambda k}, C_8^{\lambda k}, C_6^{\lambda k}, \text{and } \beta^{\lambda k}\}$, those for $k = 0$ and 1 are fundamentally defined in terms of the former and those for $k \geq 2$ in terms of the latter.

D. Truncation of the angular expansion

Since H_2 and D_2 are homonuclear, the angular expansion of Eq. (2) contains only terms with even values of λ. In all previous studies, this expansion was truncated at $\lambda = 2$; Ref. 1 experimented with the inclusion of a $P_4(\cos\theta)$ term, but could not determine it from the existing[5] data, and so omitted it. However, because of the improved resolution of the spectroscopic data now available,[6] this question is reexamined here.

TABLE II. Well depth ϵ and equilibrium distance R_e for He–inert gas potentials used to define the "collapsed diatom limit" constraint; values from Aziz (Ref. 41).

	He–Ar	He–Kr	He–Xe
ϵ/cm^{-1}	20.71	21.48	21.36
R_e/Å	3.446	3.642	3.929

From perturbation theory arguments, it is clear that a $P_4(\cos\theta)$ anisotropy will only significantly affect the eigenvalues of complexes formed from diatoms with $j \geq 2$.[1] Because of the nature of the experimental data, such contributions to the potential would be observable only for $v = 1$ complexes, so their diatom stretching dependence could not be determined here. As a result, in the fits which attempted to determine a $\lambda = 4$ anisotropy, $V_{4k}(R)$ was fixed at zero for $k \geq 2$, and $V_{41}(R)$ defined by the collapsed diatom limit constraint: $V_{41}(R) = V_{40}(R)$.

The asymptotic behavior of a $P_4(\cos\theta)$ anisotropy strength function is R^{-8}. Since the effect of such terms was expected to be relatively small, it seemed unlikely that the shape of their radial strength functions could be determined with any real precision, so no short-range exponential behavior was included. Hence, the $\lambda = 4$ anisotropy strength functions used in the present work have the simple form

$$V_{40}(R) = V_{41}(R) = -D_8(R)C_8/R^8 \tag{9}$$

while $V_{4k}(R) = 0$ for $k \geq 2$.

IV. OUTLINE OF THE FITTING PROCEDURE

Optimized values of the potential parameters were determined from direct nonlinear least-squares fits to the experimental data. The partial derivatives of the observables with respect to the independent variables, required in each cycle of the fit, were calculated numerically by first differences. In order for this approach to yield accurate derivatives, the parameter increments used to determine these derivatives should be as small as possible; if they are too small, however, the finite numerical precision of the computer introduces noise into the resulting values. A balance between these two competing sources of error was achieved by choosing the parameter increments used to define the partial derivatives such that the maximum change in the predicted value of any of the experimental observable was less than 2% of its experimental uncertainty.

In most cases, the data included in the least squares fits were weighted as the inverse square of the estimated experimental uncertainties. The two types of exceptions to this rule were the infrared transitions involving states which may undergo predissociation, and the potential anisotropy value $\overline{V}_2(R = 2.7\ \text{Å})$ introduced as a way of incorporating Buck's[17,18] inelastic differential cross sections into the present H_2–Ar analysis. While the choice of an "uncertainty" for our $\overline{V}_2(R = 2.7\ \text{Å})$ value is certainly somewhat arbitrary, a value of 2 cm^{-1} was selected, based on the sensitivity of the calculated inelastic cross sections to $\overline{V}_2$ (2.7 Å).

For infrared transitions involving metastable levels, the statistical weight used reflected both the experimental uncertainty and the uncertainty associated with the algorithm used for calculating the energies of the metastable levels. Specifically, for a level broadened by predissociation, the uncertainty in the calculated level energy is estimated to be 20% of the level width Γ. For an experimental uncertainty of magnitude u in a given line position, the (unnormalized) statistical weight used in the least squares fits was therefore: $1/[u^2 + 0.04(\Gamma_1^2 + \Gamma_2^2)]$, where Γ_1 and Γ_2 are the calculated predissociation level widths of the two levels joined by that transition.

TABLE III. Correlation matrix for the independent variables in the fits to determine the TT_3 potential for H_2–Ar. Sh (cm^{-1}) is the frequency shift parameter for the $Q_1(0)$ band of D_2–Ar.

	ϵ^{00}	R_e^{00}	β	ϵ^{01}	R_e^{01}	ϵ^{20}	R_e^{20}	ϵ^{21}	Sh
ϵ^{00}	1.00								
R_e^{00}	−0.90	1.00							
β	−0.97	0.97	1.00						
ϵ^{01}	0.78	−0.68	−0.78	1.00					
R_e^{01}	−0.82	0.87	0.84	−0.35	1.00				
ϵ^{20}	0.96	−0.94	−0.98	0.76	−0.83	1.00			
R_e^{20}	−0.89	0.76	0.84	−0.69	0.71	−0.76	1.00		
ϵ^{21}	−0.06	0.08	0.05	0.06	−0.02	−0.02	−0.01	1.00	
Sh	−0.02	0.03	0.02	−0.03	0.10	−0.02	0.04	−0.20	1.00

V. RESULTS AND DISCUSSION

A. The H_2–Ar system

The analysis for the H_2– and D_2–Ar system was the most comprehensive, in that it utilized the widest variety of experimental information. The data set consisted of all 157 uniquely assigned and unblended lines in McKellar's new infrared spectra for the H_2– and D_2–Ar complexes,[6] the 5 hyperfine transition frequencies for $H_2(v=0, j=1)$–Ar reported by Waaijer and Reuss,[15] 11 mixed virial coefficients for H_2–Ar spanning the temperature range from 77 to 323 K,[19] and a value of 164(± 2) cm^{-1} for the vibrationally averaged anisotropy strength function $\overline{V}_2$ ($R = 2.7$ Å) for ground state D_2, obtained from Buck's[17,18] inelastic cross sections in the manner described in Sec. II C. Since the absolute frequency calibration for the $Q_1(0)$ band of D_2–Ar was not as reliable as those for the rest of the new IR spectra,[43] a constant shift of the 15 lines in this band was also treated as a parameter in the fits, and was determined to be 0.0338(± 0.0073) cm^{-1}. Details of these data and the uncertainties used to define their statistical weights are summarized in Ref. 44.

The parameters characterizing our final recommended potential energy surface for molecular hydrogen with Ar are listed, together with the analogous results for the other rare gas partners, in Table I. The quantities in parentheses are the 95% statistical confidence limits in the fitted parameters; quantities for which no uncertainties are given were either held fixed at the indicated values (as were the $C_6^{\lambda k}$ values) or defined by the constraints described in Sec. III. The correlation matrix for the parameters serving as the independent variables is seen in Table III.

The quality of the agreement with experiment is indicated by the dimensionless root-mean-square deviation, defined as

$$\mathrm{RMSD} = \left\{ \left[\sum_{i=1}^{N_d} [y_{\mathrm{calc}}(i) - y_{\mathrm{obs}}(i)]^2 / u(i)^2 \right] N_d \right\}^{1/2}, \tag{10}$$

where N_d is the number of data considered. An RMSD value of $\leqslant 1$ indicates that, on average, calculations using that potential agree with the experimental data to within their uncertainties.

The most marked difference between the present surface and previous ones is in the stretching dependence of the potential anisotropy. This point is illustrated by Fig. 3, which compares the $V_{\lambda k}(R)$ radial strength functions of the present recommended TT_3 potential (solid curves) with those for one of the best earlier potentials, Carley's BC_3 surface.[2,3] Figure 3 B shows this marked change in the potential anisotropy and (particularly) in its stretching dependence, while Fig. 3 A shows that the isotropic parts of the present potential are quite similar to those of the best previous surface. Another view of the differences between these potentials is provided by Fig.4, which compares the effective anisotropy strength functions $V_2(\xi|R)$ obtained for these surfaces when the diatom bond length is fixed either at its expectation value for ground state $H_2(v=0, j=0)$ (for which $\xi = 0.0$), or at the inner ($\xi = -0.26$) or outer ($\xi = 0.33$) classical turning points of $H_2(v=1, j=2)$. While the old and new surfaces are in good agreement near $\xi = 0.0$, the

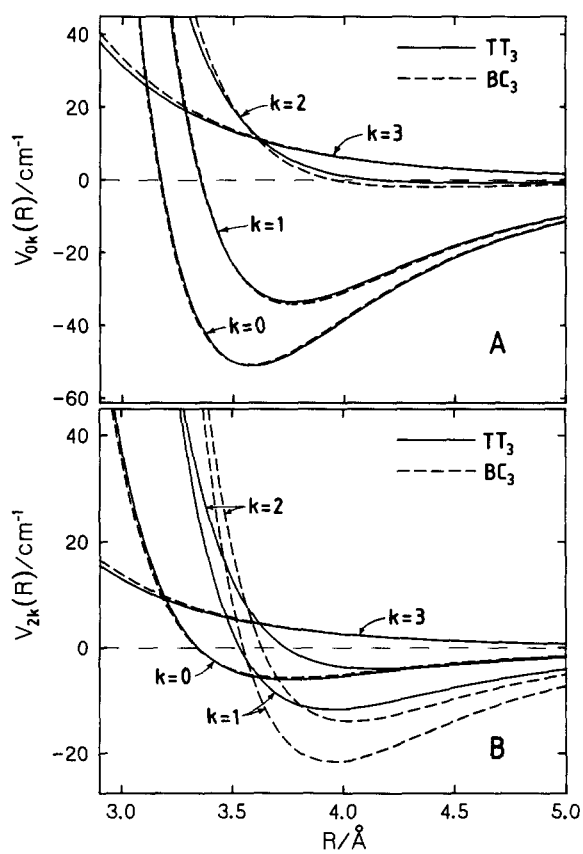

FIG. 3. Radial strength functions $V_{\lambda k}(R)$ for H_2–Ar [see Eq. (3)]: solid curves—present TT_3 surface; dashed curves—BC_3 potential of Ref. 3. Segment A—for the $\lambda = 0$ (isotropic) parts of the potential; segment B—for the $\lambda = 2$ potential anisotropy.

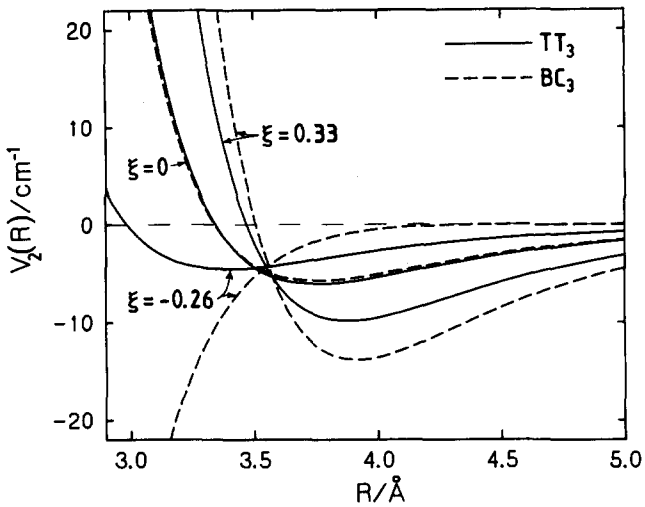

FIG. 4. Effective anisotropy strength functions for H_2–Ar corresponding to three particular values of the diatom stretching coordinate: solid curves—present TT_3 surface; dashed curves—BC_3 potential of Ref. 3.

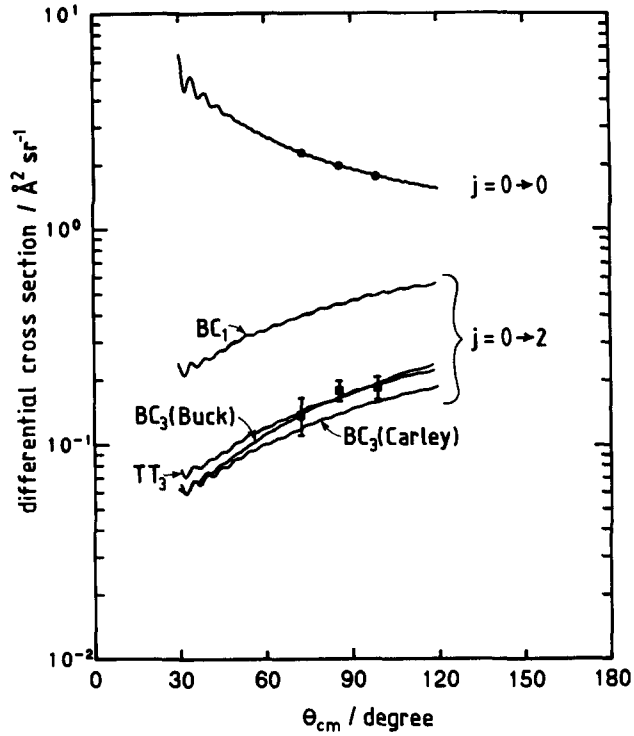

FIG. 5. Comparison with experiment (points with error bars) of elastic ($j=0\rightarrow0$) and rotationally inelastic ($j=0\rightarrow2$) cross sections predicted by various potentials for the D_2–Ar system.

$\xi = -0.26$ behavior of the present TT_3 potential is clearly much more plausibly intermediate between the well-determined region near $\xi = 0.0$ and the zero-anisotropy $\xi = -1$ limit. It thus seems clear that the BC_3 surfaces of Carley[2,3] and Buck *et al.*[18] considerably overestimated this anisotropy stretching dependence; conversely, the LJ_1 and BC_1 surfaces of Refs. 1 and 39 significantly underestimated it.

One disappointing conclusion is that it is not yet possible to discern a $\lambda = 4$ contribution to the H_2–Ar potential. An attempt was made to determine it by allowing the parameter C_8^{40} to vary in the fits. However, this led to no improvement in the quality of the fit, and the 200% relative uncertainty in the parameter value thus obtained ($C_8^{40} = -2100 \pm 4000$ cm^{-1} Å^8) clearly indicates that this contribution is too weak to be determined from the existing data.

In order to establish the credentials of our new H_2–Ar potential, it is necessary to compare its ability to reproduce a wide variety of experimental data, with those of the best previous surfaces. To this end, Table IV compares values of the dimensionless root mean square deviation [see Eq. (10)] for each of the properties considered here, calculated using four different potential surfaces. Because the infrared transition frequencies require a stretching-dependent potential to describe them even approximately, only surfaces which explicitly depend on the diatom bond length are considered.

In view of the fact that the three older potentials (the BC_1 and two BC_3 functions) were based on less accurate measurements,[5] their agreement with the new infrared data is actually remarkably good. For the hyperfine frequencies, the improvement in the quality of agreement yielded by the new potential is not surprising, since inclusion of these data in the fit is one of the key features of the present analysis; however, this change does illustrate the improved knowledge of the potential anisotropy provided by the new surface. This same comment holds for the inelastic cross sections considered in the third row of Table IV; both the present TT_3 and the Buck *et al.*[18] BC_3 functions were effectively fitted to these data, while the older surfaces were not. For this property, Fig. 5 illustrates the agreement with experi-

TABLE IV. Dimensionless root mean square deviations from experiment (RMSD) of predictions yielded by various H_2–rare gas potentials.

Rare gas	Property	Ref.	No. data	Potentials: TT_3 (present)	BC_3 (Buck, Ref. 18)	BC_3 (Carley, Refs. 3 and 4)	BC_1 (Carley, Refs. 3 and 39)
Ar	IR spectra	6	83	0.616	2.382	1.847	1.341
	HF spectra	15	5	0.479	27.44	19.2	9.75
	Inelastic cross sections	18	3	0.403	0.465	1.39	13.03
	Elastic cross sections ($13.5° < \theta_{lab} < 34°$)	18	51	0.878	1.071	1.069	1.161
	Elastic cross sections ($34° < \theta_{lab}$)	18	17	0.567	0.656	0.648	0.670
	Virials	19	11	0.635	0.712	0.712	0.793
Kr	IR spectra	6,5	70,17	0.591	···	3.499	3.861
	HF spectra	15	1	0.093	···	90.4	133.3
Xe	IR spectra	5	67	1.210	···	1.229	1.092

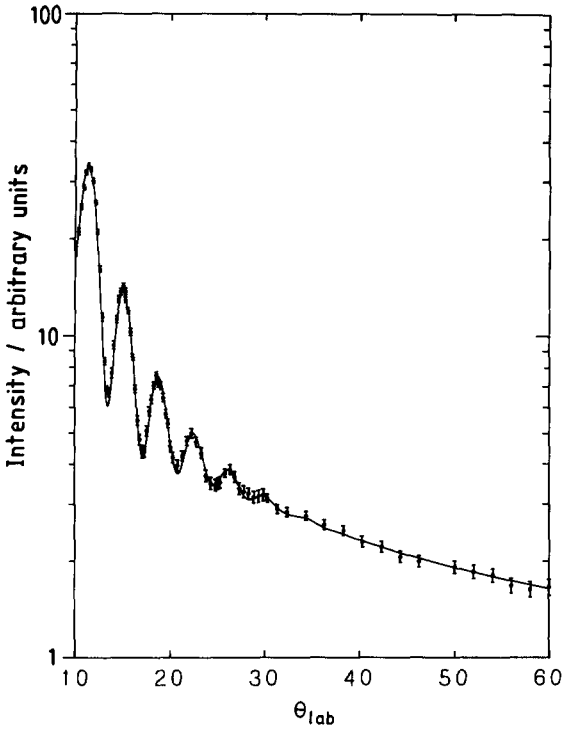

FIG. 6. Comparison with experiment (Ref. 18) (points) of the total elastic cross sections for D_2 colliding with Ar at 83.0 meV, as predicted by the present TT_3 potential.

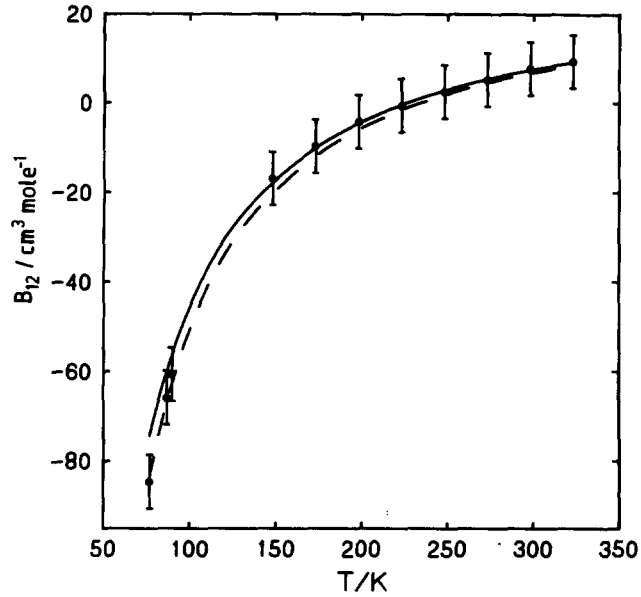

FIG. 7. Comparison with experiment (Ref. 19) (points with error bars) of virial coefficients for H_2–Ar predicted by the present potential. Dashed curve—classical calculations; solid curve—calculations performed using the first quantum correction.

this property, Fig. 5 illustrates the agreement with experiment (solid points with error bars) of the predictions yielded by the various potentials (smooth curves).

In contrast with these first three properties, Buck's[17,18] total elastic differential cross sections were not incorporated into the analysis, and hence provide an independent test of the present surface. As in earlier work,[18] separate comparisons were made for these cross sections in the oscillatory ($13.5° \leqslant \theta_{lab} \leqslant 34°$) and large angle ($\theta_{lab} > 34°$) regions, which are believed to be sensitive to different features of the potential wall. It is gratifying to note that the agreement of our predictions with experiment, illustrated by Fig. 6 and rows 4 and 5 of Table IV, is as good as that for the two-dimensional (R,θ) "$m = -3.022$" surface of Eq. (5) in Ref. 18, whose isotropic part was determined mainly from this one property.

For the virial coefficients, the analogous comparisons with experiment are shown in Fig. 7 and in row 6 of Table IV; the dashed curve in this figure was generated using a strictly classical calculation, while the solid curve was obtained on including the angular and radial first quantum corrections.[34] It is clear that the quantal corrections are quite significant for this system, particularly at low temperatures. The fact that the classical calculation agrees with experiment better than the quantal calculation is of course coincidental; it is the quantal result which properly represents the properties of the TT_3 potential.

It is clear from Table IV that the virial coefficients discriminate very little among the potential surfaces considered. Moreover, the magnitudes of the RMSD values seen there are determined mainly by the disagreement for the lowest temperature points. These values depend principally on the volume of the potential well,[33] the portion of our surface *most accurately determined* by the spectroscopic data. It therefore seems likely that the disagreement with experiment seen for the lowest temperature (77 K) point in Fig. 7 is due more to the substantial difficulty of making accurate measurements in this region than to weakness of the present potential. In retrospect, it might have been better to omit these data from the fits, but in view of the weights used this would not have resulted in a significantly different potential surface.

Another possible test of the new potential would be to compare its predictions with the infrared data now available[6] for the third isotopic species, HD–Ar. However, although the effective potential governing its dynamics has odd as well as even anisotropies, it is really nothing more than a transformed version of the H_2– and D_2–Ar surface for some intermediate values of the monomer bond length. The displaced center of mass makes the dynamics of this system much less convenient to calculate, and since these data appear to contain no new information,[45] they were not included in the present analysis.

Two more points of comparison with earlier work[18] are the questions of whether a different value of the exponent parameter β is required for the isotropic and anisotropic parts of the potential, and whether a more sophisticated form for the potential repulsion should be introduced in place of the simple exponential of Eq. (3). For both of the potential surfaces obtained in Ref. 18, the exponent parameters of the isotropic and anisotropic parts of the potential were different, and it was suggested that both this difference and the use of the more general repulsion form $R^m \exp(-\beta R)$ might be necessary to accommodate the infrared and scattering data simultaneously. The present work, however, shows that *neither* of these suggested gener-

TABLE V. Correlation matrix for the independent variables in the fits to determine the TT_3 potential for H_2–Kr.

	ϵ^{00}	R_e^{00}	β	ϵ^{01}	R_e^{01}	ϵ^{20}	R_e^{20}	ϵ^{21}	C_8^{40}
ϵ_{00}	1.00								
R_e^{00}	−0.91	1.00							
β	−0.98	0.97	1.00						
ϵ^{01}	0.68	−0.67	−0.72	1.00					
R_e^{01}	−0.95	0.94	0.96	−0.51	1.00				
ϵ^{20}	0.24	−0.24	−0.24	−0.23	−0.38	1.00			
R_e^{20}	−0.66	0.62	0.66	−0.78	0.52	0.56	1.00		
ϵ^{21}	−0.40	0.40	0.39	−0.18	0.36	0.06	0.34	1.00	
C_8^{40}	0.01	0.01	0.01	−0.09	−0.03	0.20	0.16	−0.08	1.00

alizations is required; indeed, the BC_3 potential of Ref. 18, which had different isotropic and anisotropic β values, is actually in slightly *worse* agreement with the new infrared data[6] than were the earlier potentials (although, of course, it agrees equally well with the older data[5] on which it was based). It thus appears that a simple exponential function with the same exponent parameter for all $\{\lambda,k\}$ is able to account for all the existing data for H_2–Ar.

B. The H_2–Kr system

No inelastic scattering cross sections been reported for H_2–Kr or D_2–Kr, and based on our experience with the H_2–Ar system, the available virial coefficients are expected to contain little additional information. The present analysis was therefore based on only the infrared data and the one available hyperfine transition frequency.[15] For this system, McKellar obtained new data only for the H_2 isotopic form,[6] so our analysis was based on these 53 H_2–Kr frequencies, the 17 less accurate (and appropriately weighted) D_2–Kr lines reported in the earlier work,[5] and the one hyperfine line measured by Waaijer and Reuss.[15] Further details regarding these data are presented in Ref. 44.

The parameters characterizing our recommended potential surface for molecular hydrogen interacting with krypton are listed in Table I, while the correlation matrix for the parameters varied in the fit is found in Table V. For this system it *was* found necessary to include a $P_4(\cos\theta)$ (or $\lambda = 4$) contribution to the potential anisotropy; this is the first time that such a term has been determined from experiment for any atom–diatom system. Although the C_8^{40} coefficient representing this behavior has a fairly large uncertainty, it is definitely required to explain the data, since the best fit which could be obtained when it was excluded had an overall RMSD value some 26% larger than that associated with our recommended potential. Moreover, as shown by the last row in Table V, this quantity is very weakly correlated with the other parameters fitted. Note, however, that the potential obtained from the fit which excluded $\lambda = 4$ terms is very similar to the $\lambda \leqslant 2$ portion of our recommended TT_3 potential. Of course, because of the weakness of the $V_{40}(R)$ term ($\sim -0.3\ \mathrm{cm}^{-1}$ in the region near the potential minimum), the present analysis tells us little about its functional form, and the $D_8(R)C_8/R^8$ form used here represents merely its *effective* behavior in the well region.

Because of the limited availability of appropriate data for H_2–Kr, the comparisons seen in Table IV are much less extensive than those for the Ar system. The inadequacy of the predicted hyperfine frequencies generated from the earlier potentials again illustrates both the magnitude of the model dependence which hampered the earlier analyses, and the improvement in our knowledge of the potential anisotropy for this species. Table IV also shows that the RMSD values for the infrared spectra predicted by the earlier H_2–Kr potentials are much larger than the analogous values for the Ar system. This partly reflects the fact that the Kr data were the least accurate of the 1971 measurements. However, it is probably also partly due to the increased accuracy of the new "SEPT" computational method used here,[27] an improvement which is more important for the more strongly anisotropic Kr (and Xe) complexes than for the Ar systems.

While the virial data for H_2–Kr are not sufficiently extensive to warrant detailed comparisons in Table IV, predictions generated from the present TT_3 potential agree with experiment[19] to well within the quoted uncertainties.

C. The H_2–Xe system

No hyperfine transitions or new infrared spectra have been obtained for H_2– or D_2–Xe, and no modern scattering cross sections exist for this system. As for the H_2–Kr system, the experimental virial coefficients were not used in the fits. The present analysis was therefore based solely on the (lower resolution) infrared data[5] used in previous studies.[1-4,39] The differences between the earlier analyses and the present work lie in our use of the more accurate SEPT method[27] for calculating the level energies required for simulating the spectrum, and our use of the Tang–Toennies[14] dispersion energy damping damping function of Eq. (4) in place of the simple Buckingham–Corner function used earlier. The latter change has little effect on the analysis, and even the former should not yield significant improvements, in view of the larger uncertainties in these older data. However, it does seem desirable to have a potential surface for the Xe complexes which is directly comparable to those for Kr and Ar.

The parameters of the new TT_3 potential energy surface for the H_2–Xe system are listed in Table I. As for H_2–Ar, it was not possible to determine a $P_4(\cos\theta)$ anisotropy from

the existing data. Although such terms are expected to have a larger effect on the infrared data for H_2–Xe than on those for the Kr complexes, they could not be discerned from the (lower quality) older H_2– and D_2–Xe data. On the other hand, the almost negligible differences between the $\lambda = 0$ and 2 parts of our recommended H_2–Kr potential and those for a surface obtained on omitting $\lambda = 4$ terms from the fits suggest that their absence should not in itself affect the quality of the rest of the H_2–Xe potential surface.

Since it is based solely on the lower resolution 1971 infrared data,[5] the present H_2–Xe potential is inherently less accurate than those for H_2–Kr and H_2–Ar; this point is illustrated by the magnitudes of the uncertainties in the fitting parameters seen in Table I. However, the potential anisotropy and its stretching dependence are relatively stronger for H_2–Xe than for the lighter inert gas systems, so the 1971 data[5] should determine those parts of the H_2–Xe surface more accurately than they could those for H_2–Ar or H_2–Kr. Moreover, the similarity between the pattern of the H_2–Xe parameters seen in Table I and those for the Ar and Kr systems, and the plausible nature of the trends from one system to another, also suggest that this surface should be reasonably accurate. As for H_2–Kr, predictions generated from the present TT_3 potential agree with the available experimental mixed second virial coefficients to well within the experimental uncertainties.

D. Predictions, trends and further comparisons

1. Predictions: Inelastic cross sections, predissociation lifetimes, and virial coefficients

Rotationally inelastic cross sections have not yet been measured for the H_2–Kr and H_2–Xe systems, so it is interesting to see what values are predicted for them by the present potentials. Since the reduced mass of the atom–diatom pair is almost the same for all three rare gas partners, we have performed D_2 + Kr and D_2 + Xe calculations using the same collision energy (85 meV) and experimental averaging associated with the experimental D_2 + Ar scattering[17,18] discussed above.

The large-angle elastic and inelastic differential cross sections calculated for 85 meV scattering of D_2 from Kr or Xe have the same qualitative behavior as those for D_2 + Ar (see Fig.5), but their magnitudes are different. Taking the center of mass scattering angle $\theta_{cm} = 85.5°$ (corresponding to the middle experimental point in Fig. 5) as representative, the elastic and inelastic differential cross sections (DCS) implied by our potentials for the scattering of D_2 from Ar, Kr, and Xe are presented in the first two rows of Table VI. They show that while the large-angle elastic cross sections increase with the size of the inert gas partner, the corresponding inelastic cross sections *decrease* sharply. This latter trend is *in the opposite direction* to that for the strength parameters ϵ^{2k} associated with the various components of the potential anisotropy (see Table I).

TABLE VI. Comparison of anisotropy-dependent properties of present TT_3 potentials; energies (for $\overline{V}_2$ and Γ) in cm^{-1} and differential cross sections (DCS) in $Å^2/sr$.

Property	X = Ar	Kr	Xe
D_2–X elastic DCS at 85 meV and $\theta_{cm} = 85.5°$	1.95	2.22	2.62
D_2–X inelastic DCS at 85 meV and $\theta_{cm} = 85.5°$	0.163	0.127	0.057
H_2–X RP width Γ for $(v,j,n,l,J) = (1,2,0,2,0)$	0.068	0.058	0.022
$\overline{V}_2(v=1,j=2;R_e)$ for H_2–X	−5.68	−8.29	−11.10

The level widths for rotational predissociation of complexes correlating with $j \geq 2$ are also of interest. Previous studies have shown that angular momentum coupling effects cause these widths to be different for each quantum state of a complex, with a pattern of values determined by the set of quantum numbers $\{n,l,j,J\}$.[4,30] This pattern should be qualitatively the same for all similar systems, so calculations for one representative level should define a scaling factor which can be combined with the previously published[30] results for H_2–Ar to yield reasonable predictions for the other species.

With the $(v,j,n,l,J) = (1,2,0,2,0)$ state chosen as this representative level, rotational predissociation (RP) widths were calculated from our potential energy surfaces for H_2–Ar, H_2–Kr, and H_2–Xe. For consistency with previous work,[30] these calculations were performed using the close coupling method while considering only coupling among channels corresponding to $(v,j) = (1,0)$ and $(1,2)$. Although neglect of other open and closed channels introduces small errors compared to fully converged calculations,[30,48] such errors are unimportant compared to the effect of remaining uncertainties in the potential surfaces, and have no effect on the present discussion. The level widths obtained in this way are shown in the third row of Table VI; note that their dependence on the size of the inert gas partner is qualitatively the same as that for the rotationally inelastic scattering cross sections.

The last row of Table VI lists values of the vibrationally averaged anisotropy strength function $\overline{V}_2(R)$ evaluated at the minimum of the effective isotropic potential for H_2 $(v = 1, j = 2)$. This is a measure of the effective potential anisotropy governing the level splittings and other properties of the van der Waals molecule bound states. The magnitude of this quantity *increases sharply* with the size of the inert gas partner, a change *in the opposite direction* to the trend for the inelastic cross sections and predissociation widths.

As was pointed out earlier,[4,30] this apparent contradiction between the trends in the potential anisotropy in the well region and in the inelastic cross sections results from a combination of two effects. First, as shown by Fig. 2, the inelastic cross sections and predissociation widths are sensitive to the potential anisotropy at shorter distances than are the bound state properties; secondly, as shown by Fig. 8, the changes in sign of the anisotropy strength functions for the heavier inert gas partners occur at progressively smaller distances, relative to the zeros of the associated isotropic potentials. At distances larger than the zero of the isotropic potential $(R = \sigma)$, the region to which the bound state properties are most sensitive (see Fig. 2), the effective strengths of the potential anisotropies increase in the order Ar < Kr < Xe, in

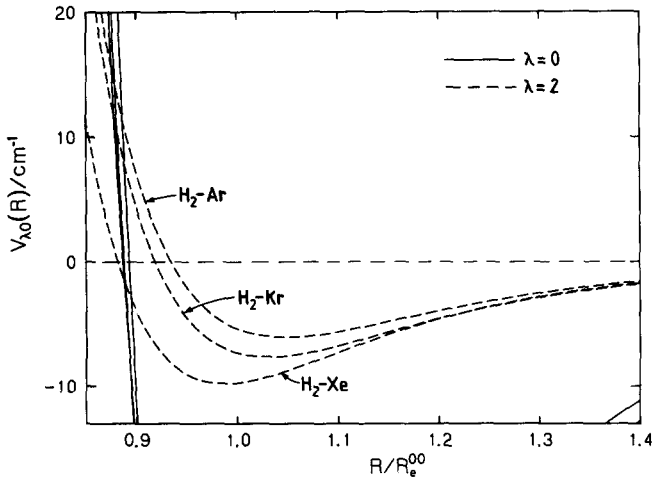

FIG. 8. Leading isotropic (solid curves) and anisotropic (dashed curves) radial strength functions $V_{00}(R)$ and $V_{20}(R)$, plotted vs the reduced distance coordinate R/R_e^{00}.

accord with the trend of the ϵ^{20} and $\overline{V}_2(v=1,j=2;R_e)$ values. Conversely, at distances smaller than $R=\sigma$, the region to which off-diagonal properties such as inelasticity and predissociation rates are most sensitive, the inward displacement of the $V_{20}(R/R_e^{00})$ curves overwhelms the effect of the increase in ϵ^{20} with size of the inert gas partner, so that the effective anisotropy strength at these smaller distances actually *decreases* from Ar to Kr to Xe.

For the leading stretching-dependent part of the isotropic potential, $V_{01}(R)$, Fig. 9 shows plots analogous to those of Fig. 8; the trends seen in Fig. 9 have physical implications similar to those in Fig. 8. In particular, since $V_{01}(R)$ has a deeper well for the larger rare gas partners, bound state properties such as the red shift of the diatom vibrational frequency on forming a van der Waals cluster or entering a rare gas matrix will increase from Ar to Kr to Xe. Conversely, the displacement of $V_{01}(R)$ to smaller distances relative to R^{00} suggests that vibrational inelasticity and vibrational predissociation widths will *decrease* with increasing size of the rare gas partner.

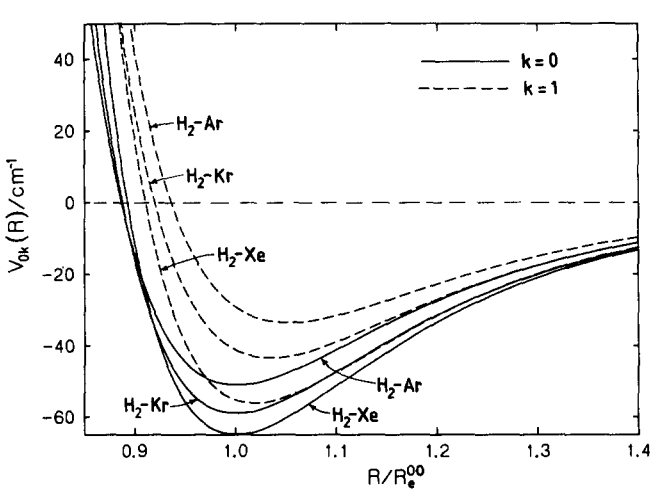

FIG. 9. Leading [solid curves, $V_{00}(R)$] and linear stretching dependent [dashed curves, $V_{01}(R)$] contributions to the isotropic potentials, plotted vs the reduced distance coordinate R/R_e^{00}.

TABLE VII. Comparison of rotational predissociation level widths Γ (in cm^{-1}) for the representative $(v,j,n,l,J)=(1,2,0,2,0)$ level of H_2–X complexes, calculated from various potential energy surfaces.

Potential energy surface	H_2–Ar	H_2–Kr	H_2–Xe
Present TT_3 surface	0.068	0.058	0.022
BC_3 surface of Carley (Refs. 2–4)	0.110	0.069	0.037
BC_3 surface of Buck *et al.* (Ref. 18)	0.186	···	···

It is instructive at this point to compare rotational predissociation level widths calculated from the present TT_3 potential surfaces with those for previously recommended potentials. For the same representative level considered above, these comparisons are summarized in Table VII.[49] It is noteworthy that the H_2–Ar BC_3 surface of Buck *et al.*[18] predicts RP widths almost a factor of 3 larger than those generated from the present TT_3 potential, in spite of the fact that these two surfaces both yield predicted inelastic cross sections in essentially exact agreement with experiment. This suggests that predissociation lifetimes may prove to be a very useful tool for determining the potential anisotropy in the neighborhood of $R=\sigma$.

Interaction second virial coefficients for mixtures of H_2 and D_2 with Ar, Kr, and Xe have been generated from the present recommended potential energy surfaces, and are listed in Table VIII. Note that the small differences between the results for the H_2 and D_2 isotopes of each species are largely due to the (positive) quantum corrections, which decrease as the reduced mass increases. In view of the quality of the present potential energy surfaces, we believe that these calculations are more accurate than the existing experimental data for these systems,[19] particularly at low temperatures.

2. Trends, and (lack of) conformal behavior

As may be seen from Table I, many of the trends in the characteristics of our potential energy surfaces with the size of the inert gas partner are in accord with intuition. In particular, as the inert gas partner becomes larger, the characteristic strength ($\epsilon^{\lambda k}$) and distance ($R_e^{\lambda k}$) parameters of the various potential components all become larger. However,

TABLE VIII. Interaction second virial coefficients $B_{12}(T)$, in cm^3/mol, generated from the potentials of Table I.

T/K	Ar + H_2	Ar + D_2	Kr + H_2	Kr + D_2	Xe + H_2	Xe + D_2
77	−74.8	−78.5	−108.8	−113.4	−144.7	−150.2
100	−45.9	−47.9	−68.3	−70.5	−90.6	−93.1
125	−28.1	−29.4	−43.8	−45.1	−58.2	−59.6
150	−17.0	−17.9	−28.6	−29.4	−38.4	−39.2
175	−9.5	−10.1	−18.3	−18.9	−25.0	−25.6
200	−4.1	−4.6	−10.9	−11.4	−15.4	−15.8
225	−0.0	−0.4	−5.4	−5.8	−8.3	−8.6
250	3.1	2.8	−1.2	−1.5	−2.7	−3.0
275	5.6	5.3	2.2	2.0	1.7	1.4
300	7.6	7.4	5.0	4.7	5.2	5.0
350	10.7	10.5	9.1	8.9	10.6	10.4
400	12.9	12.7	12.0	11.9	14.4	14.3
450	14.5	14.3	14.2	14.1	17.3	17.2
500	15.7	15.6	15.9	15.8	19.4	19.3

TABLE IX. Trends in characteristic strength and length parameters, scaled by ϵ^{00} and R_e^{00}, for the three systems.

	H_2–Ar	H_2–Kr	H_2–Xe
$\epsilon^{01}/\epsilon^{00}$	0.657	0.735	0.864
$\epsilon^{02}/\epsilon^{00}$	0.016	0.023	0.071
$\epsilon^{20}/\epsilon^{00}$	0.119	0.130	0.151
$\epsilon^{21}/\epsilon^{00}$	0.229	0.264	0.281
$\epsilon^{22}/\epsilon^{00}$	0.079	0.086	0.062
R_e^{01}/R_e^{00}	1.051	1.033	1.018
R_e^{02}/R_e^{00}	1.272	1.223	1.127
R_e^{20}/R_e^{00}	1.046	1.029	0.987
R_e^{21}/R_e^{00}	1.100	1.063	1.005
R_e^{22}/R_e^{00}	1.156	1.118	1.074

the interaction potentials for the different systems are not conformal; that is, scaling the energies by ϵ_e^{00} and lengths by R_e^{00} does not yield a common reduced potential energy surface. In particular, while the reduced rigid isotropic potentials $V_{00}(R/R_e^{00})/\epsilon^{00}$ obtained in this way are fairly similar, the corresponding angle and stretching dependent radial strength functions are markedly different. This point is clearly illustrated by Table IX, which compares scaled values of the characteristic strength and length parameters of the radial strength functions for the three systems. Conformality would be said to occur if these ratios had the same values for all three systems, and this is clearly not the case.

Another perspective on the trends among these systems is provided by Figs. 8 and 9, which show how the leading anisotropy- and stretching-dependent radial strength functions (dashed curves) are displaced to increasingly shorter distances relative to the repulsive wall of the isotropic potential (solid curves) for the heavier inert gas partners. Understanding trends of this type is quite important, since they determine the relative magnitudes of properties such as rotational and vibrational inelasticity, predissociation lifetimes, the anisotropy-induced splittings of the bound state levels, and the vibrational frequency shifts of diatomic hydrogen bound in van der Waals clusters or frozen into inert gas matrices. It should also prove useful in testing models for van der Waals interaction potentials,[7-14] and may facilitate the development of a reliable empirical stretching-dependent potential for the H_2–Ne system.

3. Form of the angular expansion

The potentials described above are all expressed, using Eqs. (1) or (2), as "linear expansions in the anisotropy of the potential" (LEAPOT). Although this type of expansion is widely used, it is by no means the only reasonable way of representing the angular behavior of a potential energy surface, and in the course of the present work considerable effort was expended testing an alternative scheme. This second approach, originally proposed by Pack,[50] is based on the use of a "linear expansion in the anisotropy of the parameters" (LEAPAR). In this formulation a radial strength function [such as Eq. (3)] is associated with each power of the internal motion stretching coordinate ξ, and its parameters are expanded as truncated Legendre expansions in the angular coordinate, such as

$$\epsilon^k(\theta) = \epsilon^{0k} + \epsilon^{2k}P_2(\cos\theta),$$
$$R_e^k(\theta) = \mathbf{R}_e^{0k} + \mathbf{R}_e^{2k}P_2(\cos\theta), \quad (11)$$

where k identifies the associated power of ξ. This type of expansion is particularly useful for interactions involving relatively long linear molecules, where the value of $R_e^k(\theta)$ changes drastically as a function of θ. For such cases, the LEAPAR form usually requires considerably fewer independent parameters than would an equivalent expansion in the traditional LEAPOT form. Moreover, use of a simple $P_2(\cos\theta)$ anisotropy for a parameter such as $R_e^k(\theta)$ implicitly introduces terms with much higher order anisotropy into the potential itself.

In the present work, the LEAPAR form was implemented using the radial strength functions of Eq. (3) with the exponent parameter β treated as independent of θ, while ϵ, R_e, and C_6 were expressed as two-term Legendre expansions with the form of Eq. (11). Independent functions of this type were introduced for $k = 0$ and 1, although by analogy with the R_e^{21} constraint described earlier we fixed $\mathbf{R}_e^{21} = \mathbf{R}_e^{20}$. The collapsed diatom limit constraint was again used to define $k = 2$ functions.

When the fits for the H_2–Ar and –Kr systems were repeated using this type of expansion, a slightly poorer quality of fit was obtained for the same number of free parameters used before. For example, use of a LEAPAR expansion which included only $P_2(\cos\theta)$ parameter anisotropies yielded an RMSD value for the H_2–Kr system of 0.806, which is slightly worse than the value 0.738 associated with the analogous LEAPOT fit. Moreover, even explicit introduction of $P_4(\cos\theta)$ anisotropy in the form of a ϵ^{40} parameter (with $\mathbf{R}_e^{40} + \mathbf{R}_e^{00}$) only reduced this value to 0.604, which is still somewhat poorer than the 0.587 associated with the recommended potential of Table I. Thus, the implicit high order potential anisotropy associated with a two-Legendre term LEAPAR expansion *did not* obviate the need to introduce an explicit $P_4(\cos\theta)$ anisotropy term for the H_2– and D_2–Kr system. We therefore concluded that use of LEAPAR-type potential expansions offers no practical advantages for the molecular hydrogen–inert gas systems, so in view of their somewhat more convenient form, LEAPOT expansions were retained as the basis of the present work.

4. Parameters characterizing vibrationally averaged potentials

The parameters tabulated in Table I fundamentally define the present recommended potential energy surfaces, and a copy of a FORTRAN subroutine for generating the TT_3 surfaces from these parameters may be obtained from the authors on request. However, in practical calculations it is the vibrationally averaged versions of these surfaces that are most relevant, since these averaged functions

$$\overline{V}(v,j|R,\theta) = \langle v,j|V(R,\xi,\theta)|v,j\rangle$$
$$= \overline{V}_0(v,j|R) + \overline{V}_2(v,j|R)P_2(\cos\theta) \quad (12)$$

define the effective potential seen by an inert gas atom inter-

TABLE X. Parameters characterizing the diagonal vibrationally averaged potentials associated with various diatom internal states; the exponent parameters β are as in Table I. Energies are in cm^{-1} and lengths in Å.

		$\lambda=0$					$\lambda=2$					$\lambda=4$
v	j	$\overline{A}^0$	$\overline{C}_8^0$	$\overline{C}_6^0$	$\overline{\epsilon}^0$	$\overline{R}_e^0$	$\overline{A}^2$	$\overline{C}_8^2$	$\overline{C}_6^2$	$\overline{\epsilon}^2$	$\overline{R}_e^2$	$\overline{C}_8^4$
						H_2–Ar						
0	0	18 888 898	1 205 256	134 534	50.88	3.5846	4 362 827	328 396	13 574	6.08	3.7563	
0	1	18 922 423	1 206 883	134 706	50.93	3.5849	4 386 254	329 836	13 618	6.10	3.7572	
0	2	18 989 414	1 210 130	135 051	51.01	3.5855	4 433 142	332 718	13 706	6.13	3.7589	
0	3	19 089 738	1 214 987	135 566	51.14	3.5864	4 503 545	337 043	13 837	6.18	3.7615	
0	4	19 223 222	1 221 438	136 248	51.31	3.5875	4 597 557	342 814	14 011	6.24	3.7648	
1	0	20 630 254	1 284 062	142 184	52.39	3.6030	5 748 484	411 717	15 660	6.81	3.8052	
1	1	20 667 230	1 285 810	142 361	52.43	3.6033	5 775 675	413 373	15 706	6.82	3.8059	
1	2	20 741 122	1 289 302	142 714	52.52	3.6040	5 830 090	416 688	15 797	6.86	3.8072	
1	3	20 851 808	1 294 525	143 240	52.64	3.6049	5 911 795	421 663	15 933	6.91	3.8092	
						D_2–Ar						
0	0	18 639 410	1 193 850	133 399	50.66	3.5819	4 167 736	316 632	13 266	5.99	3.7475	
0	1	18 655 945	1 194 656	133 485	50.68	3.5820	4 179 192	317 337	13 288	5.99	3.7480	
0	2	18 688 998	1 196 265	133 657	50.72	3.5823	4 202 112	318 748	13 331	6.01	3.7489	
0	3	18 738 537	1 198 676	133 914	50.79	3.5828	4 236 509	320 865	13 397	6.03	3.7502	
0	4	18 804 515	1 201 884	134 257	50.87	3.5833	4 282 407	323 689	13 484	6.06	3.7520	
1	0	19 840 729	1 248 527	138 796	51.74	3.5948	5 114 425	373 647	14 735	6.48	3.7852	
1	1	19 858 437	1 249 374	138 883	51.76	3.5949	5 127 162	374 426	14 758	6.48	3.7856	
1	2	19 893 835	1 251 066	139 058	51.80	3.5952	5 152 645	375 984	14 803	6.50	3.7863	
1	3	19 946 895	1 253 601	139 320	51.87	3.5957	5 190 887	378 322	14 870	6.52	3.7874	
						H_2–Kr						
0	0	24 994 784	1 898 088	190 364	58.85	3.7212	5 159 708	492 264	19 561	7.70	3.8343	11 564
0	1	25 035 348	1 900 653	190 614	58.91	3.7214	5 183 110	494 224	19 626	7.72	3.8348	11 581
0	2	25 116 389	1 905 776	191 111	59.03	3.7218	5 229 938	498 145	19 754	7.76	3.8359	11 616
0	3	25 237 721	1 913 438	191 855	59.22	3.7223	5 300 224	504 029	19 946	7.83	3.8374	11 668
0	4	25 399 094	1 923 614	192 841	59.46	3.7231	5 394 030	511 877	20 201	7.92	3.8394	11 737
1	0	27 070 632	2 022 597	201 452	61.22	3.7341	6 519 090	604 258	22 619	8.76	3.8662	12 335
1	1	27 115 122	2 025 356	201 707	61.28	3.7343	6 546 054	606 502	22 686	8.78	3.8666	12 353
1	2	27 204 015	2 030 867	202 217	61.40	3.7347	6 600 004	610 990	22 819	8.83	3.8675	12 390
1	3	27 337 137	2 039 111	202 979	61.58	3.7353	6 680 982	617 724	23 019	8.90	3.8688	12 444
						D_2–Kr						
0	0	24 696 740	1 880 071	188 720	58.49	3.7193	4 967 872	476 425	19 110	7.55	3.8289	11 451
0	1	24 716 764	1 881 341	188 844	58.52	3.7194	4 979 331	477 386	19 142	7.56	3.8291	11 459
0	2	24 756 790	1 883 880	189 093	58.58	3.7196	5 002 253	479 308	19 206	7.58	3.8297	11 477
0	3	24 816 770	1 887 682	189 465	58.68	3.7199	5 036 646	482 191	19 302	7.61	3.8304	11 503
0	4	24 896 638	1 892 742	189 960	58.80	3.7203	5 082 527	486 036	19 430	7.65	3.8315	11 537
1	0	26 130 519	1 966 446	196 540	60.19	3.7282	5 897 804	553 130	21 264	8.28	3.8528	11 990
1	1	26 151 878	1 967 782	196 667	60.22	3.7283	5 910 475	554 187	21 296	8.29	3.8530	11 999
1	2	26 194 571	1 970 452	196 920	60.28	3.7285	5 935 821	556 302	21 362	8.32	3.8535	12 017
1	3	26 258 555	1 974 452	197 298	60.37	3.7288	5 973 852	559 474	21 461	8.35	3.8542	12 043
						H_2–Xe						
0	0	58 322 151	3 332 415	268 341	64.92	3.9406	8 135 821	652 734	28 730	9.84	3.8906	
0	1	58 418 158	3 337 557	268 710	65.00	3.9407	8 163 288	654 571	28 826	9.87	3.8908	
0	2	58 610 007	3 347 829	269 447	65.16	3.9409	8 218 221	658 244	29 020	9.92	3.8913	
0	3	58 897 327	3 363 210	270 547	65.41	3.9413	8 300 601	663 748	29 309	10.00	3.8919	
0	4	59 279 633	3 383 665	272 006	65.73	3.9417	8 410 419	671 078	29 693	10.11	3.8929	
1	0	63 318 599	3 595 471	284 847	68.43	3.9495	9 666 870	751 771	33 363	11.06	3.9087	
1	1	63 424 567	3 601 109	285 226	68.51	3.9496	9 698 001	753 827	33 463	11.09	3.9090	
1	2	63 636 332	3 612 376	285 981	68.68	3.9499	9 760 259	757 935	33 665	11.15	3.9095	
1	3	63 953 559	3 629 249	287 110	68.92	3.9503	9 853 639	764 094	33 965	11.23	3.9102	
						D_2–Xe						
0	0	57 606 496	3 294 644	265 896	64.39	3.9393	7 918 588	638 618	28 047	9.66	3.8877	
0	1	57 653 841	3 297 183	266 080	64.43	3.9393	7 932 074	639 522	28 095	9.67	3.8878	
0	2	57 748 487	3 302 256	266 447	64.52	3.9394	7 959 045	641 330	28 192	9.70	3.8880	
0	3	57 890 342	3 309 860	266 998	64.64	3.9396	7 999 496	644 040	23 336	9.74	3.8884	
0	4	58 079 275	3 319 984	267 729	64.80	3.9398	8 053 424	647 651	28 528	9.79	3.8889	
1	0	61 052 895	3 476 340	277 532	66.88	3.9454	8 969 108	706 744	31 307	10.52	3.9007	
1	1	61 103 625	3 479 048	277 719	66.92	3.9455	8 983 841	707 722	31 357	10.53	3.9008	
1	2	61 205 041	3 484 459	278 094	67.00	3.9456	9 013 304	709 678	31 456	10.56	3.9010	
1	3	61 357 057	3 492 569	278 655	67.13	3.9458	9 057 497	712 610	31 604	10.60	3.9014	

TABLE XI. Parameters characterizing certain off-diagonal strength function components of the TT_3 potential for H_2–Ar and D_2–Ar (β value as in Table I). Energies are in cm^{-1} and lengths in Å.

				$\lambda=0$			$\lambda=2$		
v'	j'	v	j	$\overline{A}^0$	$\overline{C}_8^0$	$\overline{C}_6^0$	$\overline{A}^2$	$\overline{C}_8^2$	$\overline{C}_6^2$
					H_2–Ar				
0	2	0	0	18 935 518	1 207 463	134 767	4 397 086	330 491	13 637
0	3	0	1	18 996 044	1 210 300	135 066	4 442 403	333 255	13 720
0	4	0	2	19 086 830	1 214 554	135 513	4 510 454	337 406	13 844
1	0	0	0	2 588 098	124 922	13 194	1 827 376	112 133	3 378
1	2	0	0	2 221 739	101 555	10 577	1 742 388	105 731	3 108
1	1	0	1	2 592 806	125 086	13 204	1 832 589	112 432	3 382
1	3	0	1	1 983 749	86 281	8 858	1 690 031	101 721	2 931
1	0	0	2	2 969 530	148 856	15 849	1 927 762	119 423	3 661
1	2	0	2	2 602 218	125 413	13 223	1 843 010	113 030	3 390
1	4	0	2	1 752 319	71 344	7 169	1 641 620	97 949	2 758
					D_2–Ar				
0	2	0	0	18 662 938	1 194 977	133 519	4 184 627	317 668	13 298
0	3	0	1	18 693 736	1 196 443	133 675	4 207 025	319 039	13 340
0	4	0	2	18 739 919	1 198 639	133 908	4 240 639	321 097	13 403
1	0	0	0	2 143 828	104 050	11 087	1 496 673	92 026	2 828
1	2	0	0	1 928 380	90 251	9 541	1 448 458	88 359	2 672
1	1	0	1	2 145 777	104 118	11 091	1 498 827	92 150	2 830
1	3	0	1	1 787 146	81 160	8 520	1 418 193	86 025	2 570
1	0	0	2	2 365 407	118 075	12 647	1 551 282	96 062	2 990
1	2	0	2	2 149 678	104 254	11 099	1 503 137	92 397	2 834
1	4	0	2	1 648 409	72 189	7 509	1 389 701	83 796	2 469

acting with a hydrogen molecule in a particular internal state. Similarly, the off-diagonal matrix elements $\langle v,j|V(R,\xi,\theta)|v'j'\rangle$ define the corresponding coupling functions $\overline{V}_\lambda(v,j;v',j|R)$ controlling vibrational and rotational inelasticity, predissociation, and certain off-diagonal contributions to the bound state level energies. Because the angular behavior of the present potentials is represented by LEAPOT expansions, and because the exponent parameter β is independent of k, all of these effective radial functions (for the homonuclear isotopic species H_2, D_2, and T_2) retain the simple form of Eq. (3), for appropriate vibrationally averaged values of the parameters A, C_8, and C_6. (Indeed, this fact is a powerful practical argument favoring the use of the LEAPOT form.) These vibrationally averaged parameters

$$\overline{Q}^\lambda = \sum_{k=0}^{3} Q^{\lambda k}\langle v,j|\xi^k|v',j'\rangle \tag{13}$$

for $Q=A$, C_8, and C_6 may be readily calculated from the radial matrix elements and expectation values of the free diatom, $\langle v,j|\xi^k|v',j'\rangle$, which in turn may be generated from the known diatomic molecule potential energy curve using standard techniques.[51] For the convenience of the user, these vibrationally averaged parameters for a few of the most important diagonal and off-diagonal cases are listed in Tables X and XI respectively; for the diagonal case, rounded values of the secondary parameters $\bar{\epsilon}$ and $\overline{R}_e$ are also listed in Table X.

VI. CONCLUDING REMARKS

The present paper has described a multi-property analysis which yielded accurate new potential energy surfaces for the H_2–Ar, H_2–Kr, and H_2–Xe systems. For H_2–Ar and H_2–Kr, these surfaces are distinctly better defined than their predecessors[1-4] because they are largely (or wholely) based on more precise and more extensive spectroscopic data[6] than were available previously. Changes emerging from the new surfaces include particularly large improvements in our knowledge of the diatom stretching dependence of the potential anisotropy for these systems. Moreover, a distinct $P_4(\cos\theta)$ potential anisotropy term has been determined for the H_2–Kr system, the first time such a term has been obtained from experiment for any atom–diatom system.

Predictions generated from the new surfaces confirm earlier suggestions[4,30] that although the effective anisotropy strength seen by bound state properties (such as level energies) increases from H_2–Ar to H_2–Kr to H_2–Xe, properties depending on the short-range anisotropy such as rotational predissociation and rotational inelasticity *decrease* with increasing size of the inert gas partner. Analogous behavior is predicted for vibrational predissociation and inelasticity and other properties associated with the dependence of the potential energy surfaces on the diatom bond length. It is shown that these apparently conflicting trends are readily understood in terms of the details of the potential energy surfaces, and that they reflect the fact that the interaction potentials between H_2 and different inert gas partners are not conformal.

ACKNOWLEDGMENTS

We are very grateful to Dr. A. R. W. McKellar for numerous helpful discussions, to Professor U. Buck for supplying his scattering cross section program, to Dr. R. T Pack for his virial coefficient program, and to Dr. J. F. Ogilvie and

Dr. P. D. Dunlop for their comments on the manuscript. We are also pleased to acknowledge the financial support of the Natural Sciences and Engineering Research Council of Canada and the award of a Collaborative Research Grant by the NATO Scientific Affairs Division.

[1]R. J. Le Roy and J. Van Kranendonk, J. Chem. Phys. **61**, 4750 (1974).
[2]J. S. Carley, Ph.D. thesis, University of Waterloo, 1978.
[3]R. J. Le Roy and J. S. Carley, Adv. Chem. Phys. **42**, 353 (1980).
[4]R. J. Le Roy, in *Resonances in Electron–Molecule Scattering, van der Waals Complexes and Reactive Chemical Dynamics*, ACS Symp. Ser. No. 263, edited by D. G. Truhlar (American Chemical Society, Washington, DC, 1984), Chap. 13, pp. 231–262.
[5]A. R. W. McKellar and H. L. Welsh, J. Chem. Phys. **55**, 595 (1971).
[6]A. R. W. McKellar, Faraday Discuss. Chem. Soc. **73**, 89 (1982).
[7]J. W. Hepburn, G. Scoles, and R. Penco, Chem. Phys. Lett. **36**, 451 (1975).
[8]R. Ahlrichs, R. Penco, and G. Scoles, Chem. Phys. **19**, 119 (1977).
[9]K. T. Tang and J. P. Toennies, J. Chem. Phys. **66**, 1496 (1977); **67**, 375 (E) (1977); **68**, 786 (E) (1978).
[10]K.-C. Ng, W. J. Meath, and A. R. Allnatt, Chem. Phys. **32**, 175 (1978).
[11] (a) K. T. Tang and J. P. Toennies, J. Chem. Phys. **68**, 5501 (1978); (b) **74**, 1148 (1981); (c) P. Habitz, K. T. Tang, and J. P. Toennies, Chem. Phys. Lett. **85**, 461 (1982); (d) K. T. Tang and J. P. Toennies, J. Chem. Phys. **76**, 2524 (1982).
[12]A. J. C. Varandas and J. Brandao, Mol. Phys. **45**, 857 (1982).
[13] (a) C. Douketis, G. Scoles, S. Marchetti, M. Zen, and A. J. Thakkar, J. Chem. Phys. **76**, 3057 (1982); (b) W. R. Rodwell and G. Scoles, J. Phys. Chem. **86**, 1053 (1982).
[14]K. T. Tang and J. P. Toennies, J. Chem. Phys. **80**, 3726 (1984).
[15]M. Waaijer and J. Reuss, Chem. Phys. **63**, 263 (1981).
[16] (a) U. Buck, F. Huisken, J. Schleusener, and J. Schaefer, J. Chem. Phys. **72**, 1512 (1980); (b) J. Andres, U. Buck, F. Huisken, J. Schleusener, and F. Torello, *ibid.* **73**, 5612 (1980).
[17]U. Buck, Faraday Discuss. Chem. Soc. **73**, 187 (1982).
[18]U. Buck, H. Meyer, and R. J. Le Roy, J. Chem. Phys. **80**, 5589 (1984).
[19] (a) J. Brewer and G. W. Vaughn, J. Chem. Phys. **50**, 2960 (1969); (b) B. Schramm, E. Elias, and R. Pilger, Chem. Phys. Lett. **88**, 459 (1982); (c) J. Brewer, Report No. MLR-2915-C, Air Force Office of Scientific Research, No. 67-2795 (1967); (d) S. Pérez, H. Schmiedel, and B. Schramm, Z. Phys. Chem. **123**, 35 (1980).
[20]A. A. Clifford, J. Kestin, and W. A. Wakeham, Ber. Bunsenges. Phys. Chem. **85**, 385 (1981).
[21] (a) R. D. Trengove and P. J. Dunlop, Proceedings of the 8th International Symposium on Thermophysical Properties, ASME; New York (1981); (b) R. D. Trengove and P. J. Dunlop, Ber. Bunsenges. Phys. Chem. **86**, 628 (1982).
[22]P. W. Hermans, Ph.D. thesis, Universiteit Leiden, 1982.
[23] (a) J. Vitko Jr. and C. F. Coll III, J. Chem. Phys. **69**, 2590 (1978); (b) V. Chandrasekharan, M. Chergui, B. Silvia, and R. D. Etters, Physica B **131**, 267 (1985).
[24]H. Moerkerken, L. Zandee, and J. Reuss, Chem. Phys. **11**, 87 (1975).
[25]L. Zandee and J. Reuss, Chem. Phys. **26**, 327, 345 (1977).
[26]A. J. Thakkar, J. S. Carley, and R. J. Le Roy (unpublished work, 1978); results summarized in Refs. 2 and 3.
[27]J. M. Hutson and R. J. Le Roy, J. Chem. Phys. **83**, 1197 (1985).
[28]N. J. Harrick, R. G. Barnes, P. J. Bray, and N. F. Ramsey, Phys. Rev. **90**, 260 (1953).
[29]M. Waaijer, M. Jacobs, and J. Reuss, Chem. Phys. **63**, 247 (1981).
[30]R. J. Le Roy, G. C. Corey, and J. M. Hutson, Faraday Discuss. Chem. Soc. **73**, 339 (1982).
[31]J. M. Hutson and R.J. Le Roy, J. Chem. Phys. **78**, 4040 (1983).
[32]H. Kreek and R. J. Le Roy, J. Chem. Phys. **63**, 338 (1975).
[33]J. O. Hirschfelder, C. F. Curtiss, and R. B. Bird, *Molecular Theory of Gases and Liquids* (Wiley, New York, 1964).
[34]R. T Pack, J. Chem. Phys. **78**, 7217 (1983).
[35]J. M. Hutson and F. R. McCourt, J. Chem. Phys. **80**, 1135 (1984).
[36]J. M. Hutson, J. Chem. Phys. **86**, 854 (1987).
[37]W.-K. Liu and F. R. McCourt, Chem. Phys. **27**, 281 (1978).
[38] (a) H. Kreek and W. J. Meath, J. Chem. Phys. **50**, 2289 (1969); (b) H. Kreek, Y. H. Pan, and W. J. Meath, Mol. Phys. **19**, 513 (1970).
[39] (a) R. J. LeRoy, J. S. Carley, and J. E. Grabenstetter, Faraday Discuss. Chem. Soc. **62**, 169 (1976); (b) J. S. Carley, *ibid.* **62**, 303 (1976).
[40]R. A. Aziz, in *Inert Gases*, Springer Series in Chemical Physics, Vol. 34, edited by M. L. Klein (Springer, Berlin, 1984), Chap. 2, pp. 5–86.
[41]R. A. Aziz (private communication, 1985).
[42]K. T. Tang, J. M. Norbeck, and P. R. Certain, J. Chem. Phys. **64**, 3063 (1976).
[43]A. R. W. McKellar (private communication, 1984).
[44]R. J. Le Roy and J. M. Hutson, University of Waterloo Chemical Physics Research Report CP-287 (1986).
[45]The apparent inconsistency (Ref. 32) of the early HD–Ar data (Ref. 46) with a potential determined (Ref. 1) from the spectra for H_2– and D_2–Ar was later found to be due to inadequacies in the early HD–Ar calculations (Ref. 3). Moreover, the agreement between the new HD–Ar data (Ref. 6) and frequencies generated (Refs. 31 and 47) from the best previous potential (the BC_3 surface of Ref. 3) is well within the experimental uncertainties.
[46]A. R. W. McKellar, J. Chem. Phys. **61**, 4636 (1974).
[47]I. F. Kidd and G. G. Balint-Kurti, Chem. Phys. Lett. **105**, 91 (1984).
[48]I. F. Kidd and G. G. Balint-Kurti, J. Chem. Phys. **82**, 93 (1985).
[49]Note that the widths for H_2–Kr and Xe now calculated from the BC_3 surfaces of Carley and Le Roy (Refs. 2–4) differ slightly-from those quoted in Refs. 4 and 30, because of a minor computational error in the earlier work.
[50]R. T Pack, Chem. Phys. Lett. **55**, 197 (1978).
[51]C. Schwartz and R. J. Le Roy, J. Mol. Spectrosc. (in press).